

DGNet: Dynamic Gradient-guided Network with Noise Suppression for Underwater Image Enhancement

Jingchun Zhou¹, Zongxin He¹, Dehuan Zhang¹, Kin-man Lam², Weishi Zhang¹, Xianping Fu¹,
Yi Wang², Chongyi Li³

¹ Dalian Maritime University, ² Hong Kong Polytechnic University, ³ Nankai University

Abstract

Underwater image enhancement (UIE) is a challenging task due to the complex degradation caused by underwater environments. To solve this issue, previous methods often idealize the degradation process, and neglect the impact of medium noise and object motion on the distribution of image features, limiting the generalization and adaptability of the model. Previous methods use the reference gradient that is constructed from original images and synthetic ground-truth images. This may cause the network performance to be influenced by some low-quality training data. Our approach utilizes predicted images to dynamically update pseudo-labels, adding a dynamic gradient to optimize the network's gradient space. This process improves image quality and avoids local optima. Moreover, we propose a Feature Restoration and Reconstruction module (FRR) based on a Channel Combination Inference (CCI) strategy and a Frequency Domain Smoothing module (FRS). These modules decouple other degradation features while reducing the impact of various types of noise on network performance. Experiments on multiple public datasets demonstrate the superiority of our method over existing state-of-the-art approaches, especially in achieving performance milestones: PSNR of 25.6dB and SSIM of 0.93 on the UIEB dataset. Its efficiency in terms of parameter size and inference time further attests to its broad practicality. The code will be made publicly available.

1. Introduction

In recent years, deep learning-based methods have demonstrated their efficient computation and outstanding performance, leading to their widespread applications in computer vision, such as image denoising [12], deblurring [4, 45, 52, 53], dehazing [6, 24, 37], deraining [2, 10, 11], desnowing [29, 35], and enhancing images under low-light conditions [18, 19, 38, 47]. Deep learning makes significant breakthroughs. The advancements achieved in these ar-

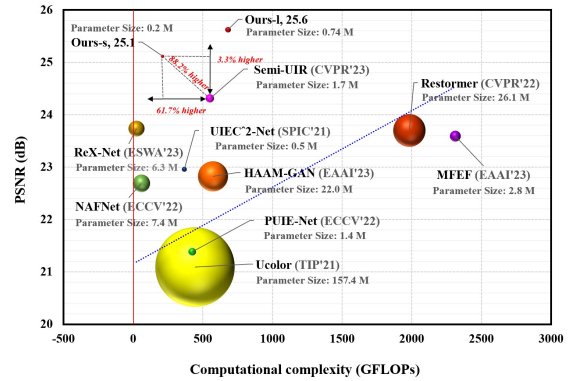


Figure 1. Performance comparison between state-of-the-art methods [1, 5, 8, 17, 34, 41, 43, 44, 51] and our methods on the UIEB V90 dataset [15]. Evaluation metrics include PSNR for image quality, computational complexity (GFLOPs), and parameter size represented by ball size. Our method achieves remarkable performance milestones.

eas markedly elevate the visual quality of images captured under adverse conditions, significantly bolstering the efficacy of downstream applications, such as object detection, classification, and image matching. However, most existing methods focus on specific types of image degradation, while underwater image enhancement (UIE) involves multiple degradation factors, such as noise, marine snow, and low-light conditions. This makes UIE more challenging and complex than single-degradation image enhancement.

Due to the involvement of multiple degradation factors, underwater degradation scenes are complex. The water medium absorbs and scatters, causing underwater images to have high noise levels, uneven illumination, low contrast, blurred details, and color shifts, among other visual problems [49, 50]. These issues make it challenging to obtain clear optical information for underwater exploration tasks, which is a challenge for both human vision and computer vision. Most of the current deep learning-based UIE methods use supervised learning frameworks. These methods require paired datasets to learn the mapping from degraded

images to clear images. However, due to the limitations of optical devices and the complexity of underwater imaging, obtaining clear underwater images or ideal reference images for restoration is a challenging task. Existing methods based on synthetic datasets suffer from the following issues. **(1) Limited paired real data:** artificially synthesized degraded images may not capture the full diversity and complexity of real underwater scenes [21]. These synthetic images cannot accurately simulate the real underwater conditions. Therefore, models trained using synthetic data cannot handle unseen or challenging underwater scenarios well. **(2) Unpredictable misdirection:** using the best results from existing enhancement methods as ground truth [15]. This approach limits supervised learning methods to the performance of existing enhancement methods. It may also introduce unwanted semantic features and distort the original characteristics of the images [33], resulting in models that cannot generalize well to real-world underwater images. These issues show the difficulties in creating datasets for UIE and the potential drawbacks of relying only on existing data for supervision.

In order to mitigate the impact of low-quality data in the dataset and address the complex degradation factors present in different underwater scenarios, we propose a novel method called DGNet, which stands for Dynamic Gradient-guided Network for UIE. The core idea of DGNet involves the use of self-updating pseudo-labels to construct additional dynamic gradients, coupled with the supervision of reference gradients in the backward propagation process. During the training process, these pseudo-labels are generated using the Contrast Limited Adaptive Histogram Equalization (CLAHE) method, imparting sensitivity to illumination and contrast changes. This sensitivity guides the network to focus more deeply on the fundamental causes of image degradation, extending beyond the constraints imposed by reference ground truth images. Moreover, the dynamic gradient adjusts the gradient space after each iteration, facilitating the network to escape the constraints of saddle points in the gradient space, which allows it to explore a broader solution space.

Furthermore, when confronted with the challenge of image enhancement under the influence of noise, we design two innovative modules to collectively mitigate the impact of various types of noise. Firstly, the Feature Restoration and Reconstruction module (FRR) eliminates irregular noise and other degradation factors by reconstructing the overall distribution of features, effectively addressing the majority of degradation issues. Secondly, the Frequency Domain Smoothing module (FRS) smooths motion noise and low-frequency features. By initially extracting high-frequency features, it guides attention to the low-frequency region, smoothing color variations in that region and alleviating issues such as artifacts. The experi-

mental results on the UIEB dataset, a public benchmark, show that our methods, Our-S (0.2M parameters, suitable for severely arithmetic-limited scenarios) and Our-L (0.7M parameters) achieve PSNR scores of 25.1dB and 25.6dB, respectively. These scores largely surpass the current state-of-the-art methods. Additionally, our methods have better parameter size and computational efficiency than the state-of-the-art methods (see Fig. 1 and Tab. 1). This suggests their high generalization potential and broad applicability.

The contributions of this paper are summarized below.

(1) We present DGNet, a Dynamic Gradient-guided Network for UIE. Our network incorporates a pseudo-label strategy to construct additional dynamic gradients, guiding the network to delve deeper into the fundamental causes of image degradation. This enables DGNet to adapt to diverse scenarios. Furthermore, the pseudo-labels dynamically adjust the gradient space after each epoch, providing the network with increased momentum during a training cycle, and facilitating its exploration of a broader gradient space to seek optimal solutions.

(2) We design multiple modules to address the impact of noise. Unlike other denoising methods that are specifically tailored to address certain types of noise, our modules are not designed to tackle specific noise types. Instead, they focus on eliminating all degradation factors that deviate from the overall distribution. Consequently, these modules do not introduce additional parameters or computational load, ensuring the network’s broad applicability and lower risk of overfitting.

(3) Our network features a simple and efficient architecture with a low parameter size, designed to address the practical challenges of underwater environments. Our small model operates at a processing speed of 26.3 frames per second for 480P images on an RTX 3090 GPU, achieving high efficiency without compromising performance.

2. Related Work

2.1. Underwater Data-Driven Strategies

The key to underwater vision tasks lies in how to acquire authentic and diverse semantic information, which is heavily dependent on the quality of existing underwater datasets. Existing underwater datasets can be categorized into two types: artificially synthesized [16] and authentically collected [29]. The artificially synthesized datasets mostly consist of manually generated degraded terrestrial scenes, offering advantages such as abundant quantity and simple label creation. In contrast, authentically collected data can reflect the real rules of underwater imaging, but their quality is affected by the manual labeling process, and they are costly to acquire.

Based on the utilization of datasets, deep learning-based image enhancement methods can be classified into unsuper-

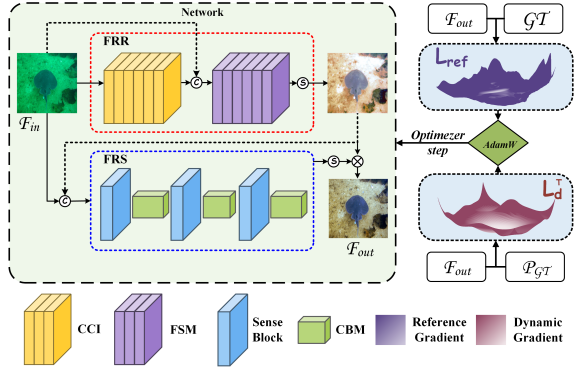


Figure 2. Overall structure of DGNet. The FRR deals with noise and other degradation factors, while the FRS module smooths features. FRR consists of Channel Convolution Inference (CCI) and Feature Smoothing Module (FSM) (detail in Fig. 3). We construct a dynamic gradient with the predicted image, which along with the reference gradient, jointly supervises the network. The CBM consists of a convolutional, BN layer with MiSH activation function.

vised, semi-supervised, and fully supervised approaches. Unsupervised methods like WaterGAN [21] and HybrUR [43] employ Generative Adversarial Networks (GANs) to simulate realistic underwater scenes, alleviating the high cost of dataset creation. The semi-supervised Semi-UIR [9] method integrates supervised and contrastive learning, utilizing both labeled and unlabeled data for image enhancement. Supervised methods [7, 17, 42] are limited by the distribution and quality of datasets, leading to suboptimal performance in specific scenarios.

The effectiveness of UIE methods is constrained by the quality of datasets, making it challenging to address this issue through data acquisition methods alone. Unsupervised approaches have trouble verifying the accuracy of the learned imaging relationships, while supervised approaches suffer from fitting errors due to low-quality real data.

2.2. Lightweight and Effective UIE Method

UIE is a crucial task for underwater exploration robots, which have limited computational resources that they also need for other functions. Traditional methods [14, 28, 32, 42, 46] achieve favorable results in specific scenarios. They usually separate the degradation process into steps based on color bias, noise, and brightness, but do not consider how enhancements affect computer vision perception. Deep learning-based methods generally use underwater imaging models to describe the imaging mechanism, focusing on subjective factors like color bias and brightness, while neglecting noise issues caused by backscattering. Some methods use data augmentation to deal with noise, but most of them do not match the real noise conditions well.

In summary, many approaches fail to improve complex situations that involve several interrelated deterioration fac-

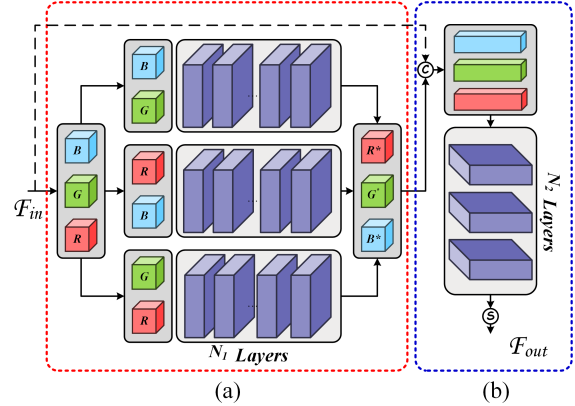


Figure 3. Detail in FRR module. (a) Channel Combination Inference (CCI). (b) Fusion Sense Module (FSM). The blue block is the CBM that consists of a convolution, BN layer with MiSH activation function. In the CCI block, we replace normal convolution with group convolution.

tors. They focus on prominent factors like brightness and color bias, neglecting the impact of noise on machine vision. Some methods with high parameter sizes [27] or low efficiency are ill-suited for underwater conditions.

3. Proposed Method

In this section, we describe our network and components, where the FRR module adept at addressing complex degradation factors (e.g., irregular noise, illumination, color bias, etc.), while the FRS module is used to deal with remove motion noise occurring underwater to avoid artifacts, and to accelerate the training of the network to cope with the low-quality images in the dataset by using dynamic gradients constructed from pseudo-labels to direct the network’s attention to the deep degradation features.

3.1. Feature Reconstruction and Re-Learning

Underwater degradation factors are complex and varied, making it challenging for networks to adapt their diverse characteristics. Most existing underwater methods tend to ignore noise [3, 31], or use more computational resources to learn the noise distribution [40]. In practical training, the networks with large amounts of parameters can lead to overfitting. We think that this inefficient strategy fails to eliminate erroneous representations and does not serve downstream high-level vision tasks effectively.

To address the above issues, we propose an innovative channel pixel inference strategy, analyzing the underwater imaging model and the image sampling mechanism. In the RGB image, each channel represents the same scene with different statistical characters. When there is no noise interference, the feature expression conforms to the light attenuation model; otherwise, undesired features are introduced

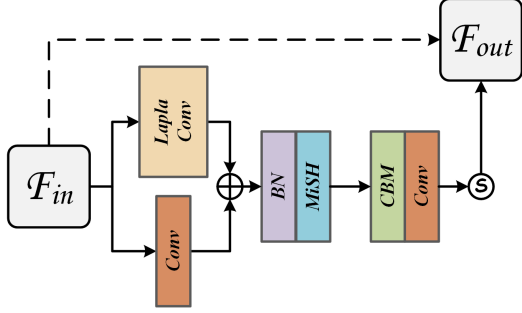


Figure 4. Structure of Sense block. Featuring LaplaConv with fixed-weight laplace convolution.

into the RGB channels. Our designed channel pixel inference strategy takes advantage of this characteristic, that is, any pixel point other than the primary colors should simultaneously exist in two channels. When we remove a certain channel pixel, the network infers the true pixel through the learned attenuation model. Even for primary color pixels, which only exist in one channel, the network can simply infer them from the adjacent local area.

We propose a novel Channel Combination Inference Block (CCI) based on this strategy, which infers the true pixels of all three channels by using pairwise combinations between channels. The CCI block’s structure is shown in Fig. 3 (a). Given an input image F_{in} of size $[B, C, H, W]$, its convolutional combinations have a receptive field that is neither too local nor too global, matching our strategy of ‘inferring and restoring primary color pixels from the neighboring regions’. The following equations describe the CCI block:

$$F_{combin} = Concat([F_{in}, F_{in}]) \quad (1)$$

$$C_{fix} = GCB_{g=3, N_1}(F_{combin}) \quad (2)$$

$$B_{fix} = Concat([C_{fix}, F_{in}]) \quad (3)$$

where GCB denotes N_1 grouped convolutional combinations, with the number of groups set to 3, corresponding to the number of channels that need to be inferred (as RGB images have 3 channels); σ denotes the Mish activation function. The inferred reconstructed pixels C_{fix} are concatenated with the original pixels to yield the final output tensor B_{fix} . We opt for concatenation instead of addition because the grouped convolutions inhibit the interchange of gradient information; thus, we cannot fully execute the ‘inference and restoration of primary color pixels from the neighboring regions.’ The network does not truly obtain local features that encompass all three RGB channels, which is specifically validated by subsequent ablation studies. We use concatenation to complete the final restoration in the subsequent stage module, with the entire strategy summa-

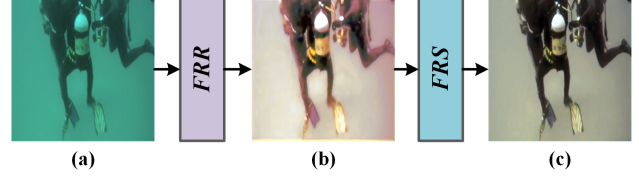


Figure 5. Comparative visualization: (a) original image, (b) images processed by FRR module, and (c) images processed by FRS module. (b) and (c) are generated by the proposed DGNNet. They could be noticed that the FRS-processed image reduces the artifacts.

rized as follows:

$$B_{fix} = Concat(R'G'B', RGB) \quad (4)$$

$$F_{out} = CBM_{N_2}(B_{fix}) \quad (5)$$

where N_2 is the number of CBM block in FSM block. Degradation factors such as irregular noise will be removed after the FRR module.

3.2. Smoothing High-frequency Laplacian

UIE is a challenging task because of the complex noise and the lack of clear paired underwater datasets. The water body can also distort the image features when the camera or the photographer moves. This makes some pixels deviate from their actual position, creating a diffusion effect, especially in the deep sea where this phenomenon is more severe. This impairs the faithful representation of pixel features and introduces artifacts, but existing methods cannot cope with it. As a result, the enhancement quality and accuracy for handling highly degraded images are limited.

To a certain extent, such disturbances in feature distribution can lead to the appearance of artifacts in the enhanced image, as shown in Fig. 5 (b). We propose a new method to smooth the low-frequency regions of the features affected by artifacts, using the Laplacian operator. This method restores the feature distribution to match the real scene, the structure of Sense block (base components of FRS) is shown in Fig. 4.

The input image F_{in} is processed through a fixed-weight Laplacian operator convolution kernel, which assigns greater weight to high-frequency features, denoted as:

$$F_{high} = F_{in} \times w \quad (6)$$

$$w = \begin{bmatrix} 0 & 1 & 0 \\ 1 & -4 & 1 \\ 0 & 1 & 0 \end{bmatrix} \quad (7)$$

where w represents the weight of the Laplacian.

The obtained high-frequency area is subtracted from a feature map extracted by a 3×3 convolution, using tensor subtraction to generate a low-frequency attention map A .

This low-frequency attention map is then sent to a convolutional group to perform feature smoothing. Finally, the low-frequency map, weighted by a Sigmoid function, is added to the original input F_{in} to produce the final smoothed image S .

$$F_{normal} = CBM(F_{in}) \quad (8)$$

$$A = Mish(BN(F_{normal} - F_{High})) \quad (9)$$

$$S = F_{in} + Sigmoid(Conv(CBM(A))) \quad (10)$$

In summary, we analyzed the characteristics of water body oscillations and designed the use of a fixed-weight Laplacian operator to operator to flat-separate high-frequency features in the real world from the spectral domain and smooth the remaining portion of the features. This approach allows for a more accurate interpretation of object edges, ensures smoother transitions of image colors, and solve the problem of edge artifacts after deep-sea image enhancement, as shown in Fig. 5.

3.3. Auto-updating Pseudo-labeling Strategy

Acquiring paired underwater datasets is challenging, and synthetic underwater images lack realism. To overcome the misleading guidance of datasets, we developed a data augmentation method that combines pseudo-labels with paired data. This method applies CLAHE to generate pseudo ground truth (GT) for each predicted image. During the gradient backpropagation process, the pseudo GT produced by the CLAHE-enhanced (CLAHE method helps to improve contrast and balance lighting, which can provide deeper features to the network.) network accentuates features such as light balance, contrast, and more. Simultaneously, it introduces a dynamically guided gradient for image generation, facilitating the network’s escape from saddle points in the gradient space and mitigating the negative impact of low-quality GT.

Relying only on pseudo-labeled constraint networks might cause incorrect gradients. Hence, our pseudo-labeling strategy is more like adding a direction marker to the existing gradient space, rather than the self-supervised method of using only pseudo-labels. In particular, we apply CLAHE operations to the network prediction image F_{pred} to generate pseudo-labels under the current gradient. As a result, the pseudo-label is updated after each gradient descent, and the dynamic gradient it generates evolves. Together with the reference gradient, it forms a continuously updated complete gradient space. This aids the network in building momentum away from saddle points, all the while offering a broader solution space. CLAHE creates pseudo-

labels as follows:

$$I_s = Split_t(I) \quad (11)$$

$$I_s^e = HE(I_s) \quad (12)$$

$$E = Concat(I_s^e) \quad (13)$$

$$P_{gt} = Clip(E) \quad (14)$$

where we define the pseudo-labels P_{gt} as the result of applying histogram equalization to the enhanced images E , t is set to 8, and $Clip$ restricts the range of the pixel values.

Instead of using the original or the real image, the pseudo-label is based on the predicted image. This approach makes pseudo-label gradient changes as the model weights update, which prevents the network from getting stuck in local optima. Moreover, since CLAHE usually improves the white balance of the image, and white balance is a key feature of the ground image, our pseudo-label also guides the prediction of white balance in multiple training rounds. This enhances the correct gradients that align with the desired white balance while diminishing the impact of incorrect ones. Our experiments show that this label generation method not only speeds up network training but also increases accuracy (detail in supplementary material).

3.4. Loss Function

We propose two gradient spaces for guiding the training of the network and improving the accuracy of the network:

- **Reference gradient:** L_1 loss function is primarily used to assess the prediction error loss between each pixel of the predicted image and the reference image, and it is a part of the reference gradient. L_{SSIM} loss primarily assesses the similarity [36] between the predicted image and the reference ideal image, providing gradients of luminance, contrast, and structure for the reference gradient.

- **Dynamic gradient:** Dynamic Tuning Loss L_d^T is primarily used to dynamically adjust the gradient space of the network. It performs the establishment of pseudo-GT on dynamic predicted images and uses MAE (Mean Absolute Error) to evaluate the pixel-level loss between the predicted images and the pseudo-GT images which spawn by Eqs. (11), (12), (13), and (14).

$$L = \alpha \cdot L_1 + \beta \cdot L_{SSIM} + \gamma \cdot L_d^T \quad (15)$$

where α , β , and γ is the weight of each loss.

To maximize the effectiveness of the L_d^T , during the initial phase of training, the weight of L_d^T should be less than that of L_1 , with the reference gradient dominating the training process. As training progresses, the influence of the reference gradient gradually diminishes, and the dynamic gradient increasingly guides the network. When the network becomes stuck in a local optimum, L_d^T will reconstruct the dynamic gradient based on the current gradient predictions



Figure 6. Visual comparison of different methods on UIEB, U45, and UCCS datasets. The visual comparison of different methods from left to right includes UWCNN[16], SMLB[31], UIEC²-Net[34], Ucolor[17], PUIE-Net(MC)[5], PUIE-Net(MP)[5], NAFNet[1], Restormer[41], MFEF[51], Semi-UIR[8], HAAM-GAN[43], Rex-Net[44], and Our method.

to help the network escape the local optimum without incurring excessive resource costs, thereby quickly converging to a global optimum. Additionally, the dynamic direction of L_d^T always points towards white balance, ensuring that the predicted image’s lighting and high-level semantic features on the RGB channels are in line with real-world scenes.

4. Experiments

In this section, detailed information about the experimental setup and analysis of the comparison with state-of-the-art methods is provided. More details on experiments, such as color constancy verification experiments based on the Grey

World Theory [48], are provided in the Supplementary Materials.

4.1. Implementation Details

In our implementation, the proposed DGNet is divided into two models: Our-s (a small model with $N_1 = 3$ and $N_2 = 3$) and Our-l (a large model with $N_1 = 6$ and $N_2 = 6$) designed for different computational devices and task scenarios, as shown in Fig. 3. The experiments were conducted on a system running Ubuntu 20.04 with an Intel Xeon Gold 6330 CPU and an RTX 3090 24GB GPU. The software package was built using Python 3.10 and PyTorch

Methods	UIEB V90					UIEB C60		UCCS		U45		Z700	
	PSNR↑	RMSE↓	SSIM↑	UCIQE↑	UIQM↑	UCIQE↑	UIQM↑	UCIQE↑	UIQM↑	UCIQE↑	UIQM↑	UCIQE↑	UIQM↑
SMBL(TB'20)[31]	16.681	0.158	0.801	0.604	2.552	0.584	2.006	0.549	2.552	0.602	2.416	0.561	3.084
UWCNN(PR'20)[16]	17.949	0.134	0.847	0.546	3.033	0.520	2.546	0.498	3.025	0.546	3.079	0.508	2.974
UIEC ² -Net(SPIC'21)[34]	22.958	0.078	0.907	0.600	3.013	0.584	2.611	0.544	2.992	0.608	3.145	0.577	2.996
Ucolor(TIP'21)[17]	21.093	0.096	0.872	0.580	3.048	0.553	2.482	0.550	3.019	0.573	3.159	0.550	3.059
PUIE-Net (MC)(ECCV'22)[5]	21.382	0.093	0.882	0.582	3.049	0.558	2.521	0.536	3.003	0.578	3.199	0.562	3.075
PUIE-Net (MP)(ECCV'22)[5]	18.257	0.126	0.778	0.569	3.064	0.513	2.398	0.489	2.758	0.563	3.186	0.548	3.083
NAFNet(ECCV'22)[1]	22.691	0.080	0.870	0.592	3.044	0.559	2.751	0.544	2.913	0.594	3.087	0.571	3.011
Restormer(CVPR'22)[41]	23.701	0.073	0.907	0.599	3.015	0.570	2.688	0.546	2.980	0.600	3.097	0.576	3.073
MFEF(EAAI'23)[51]	23.589	0.073	0.918	0.600	3.062	0.566	2.652	0.556	2.977	0.606	3.157	0.584	2.981
Semi-UIR(CVPR'23)[8]	24.309	0.073	0.901	0.605	3.032	0.583	2.663	0.557	3.079	0.606	3.185	0.591	2.900
ReX-Net(ESWA'23)[44]	23.734	0.073	0.910	0.598	2.980	0.570	2.654	0.540	2.897	0.597	3.128	0.573	3.058
HAAM-GAN(EAAI'23)[43]	22.824	0.080	0.882	0.602	3.169	0.570	2.876	0.556	3.029	0.606	3.172	0.578	2.998
Our-S	25.067	0.071	0.925	0.611	3.100	0.592	2.731	0.565	3.016	0.607	3.219	0.595	3.089
Our-L	25.623	0.069	0.929	0.610	3.081	0.592	2.736	0.569	3.011	0.610	3.212	0.593	3.061

Table 1. Quantitative method comparisons across UIEB, UCCS, U45, and Z700 datasets. Top performances highlighted: best in Red, second in blue.

2.1.0 with CUDA 11.8 support.

The Exponential Moving Average (EMA) strategy was employed, and the input size was gradually increased from 256×256 to 400×400 during training to enhance the model’s generalization capability. The Adamw optimizer was chosen, and the learning rate was set to $1e-3$ with a batch size of 5 under global seed 0.

4.2. Datasets and Evaluation Metrics

We used four publicly available datasets as benchmarks in our experiments: UIEB [15], U45 [20], UCCS [23], and Z700. The UIEB dataset consisted of 890 real underwater images with synthetic references and 60 unpaired real images (C60). The U45 and Z700 datasets contained 45 and 700 realistic underwater scenes, respectively. The UCCS dataset comprised real images from three scenes: 100 blue-shifted, 100 green-shifted, and 100 blue-green-shifted. We divided the paired data in the UIEB dataset into a training set of 800 images (T800) and a validation set of 90 images (V90). T800 served as the training set, V90 as the validation set, and the other datasets were used as test sets for all the methods.

To comprehensively evaluate the performance of the proposed DGNNet, we adopted three reference metrics: Mean Squared Error (MSE), Peak Signal-to-Noise Ratio (PSNR) [13], and Structural Similarity (SSIM) [36], to measure the differences between the enhanced images and the reference images. Additionally, we employed two widely used no-reference metrics: Underwater Image Quality Measure (UIQM) [26] and Underwater Color Image Quality Evaluation Metric (UCIQE) [39], to quantify color smoothness, clarity, and contrast. To further assess the practical performance of the model, we measured the frame rate (The FPS results are displayed in the Supplementary Material.) for inferring HD images on an RTX 3090, which indicates the inference speed of the model.

4.3. Comparison with SOTA Methods

4.3.1 Qualitative Comparisons

Visual comparisons of our method (Our-L) and 12 other SOTA methods are presented in Fig. 6. We selected representative scenes from four datasets that cover a wide range of real underwater scenarios. Our method effectively corrects color casts and exhibits higher saturation in the V90 dataset. Our method outperforms other methods in terms of preserving details in the C60 dataset. The second row demonstrates the consistent performance of our method in haze removal for objects at different distances. The third row shows that our method, along with UIEC²-Net, achieves better restoration results for the given scene. Our method proves to be effective in various color-shifted scenes in the UCCS dataset. In the first scene of U45, only our method, Semi-UIR, HAAM-GAN, and Rex-Net reasonably restore the red and green colors of the bottom vegetation. However, HAAM-GAN exhibits grid patterns, while Rex-Net shows overcompensation in red. In the second scene, our method successfully restores object edges and color shifts. In the third scene, our method accurately restores the original colors of the beach, while the other methods exhibit unrealistic color rendering.

4.3.2 Quantitative Comparisons

As displayed in Tab. 1, our method achieves a quantitative comparison with 16 SOTA methods. Both the Our-S and Our-L models obtain higher values across various metrics, significantly surpassing other SOTA methods. On the UIEB C90 dataset, compared to Semi-UIR (CVPR’23), our Our-L models demonstrate improvements of 5.4% in PSNR and 3.1% in SSIM, respectively. Additionally, as observed from Fig. 1, our method exhibits lower parameter size and computational complexity, making it suitable for practical applications.

Operation		PSNR	SSIM	UIQM	UCIQE
Instead ALL		15.892	0.732	1.780	0.595
FRR	w/o CCI	25.231	0.925	3.073	0.608
	w/o FSM	23.164	0.916	3.055	0.601
	w/o Sigmoid	24.869	0.922	3.045	0.604
	Remove	24.916	0.922	3.077	0.610
	Instead	16.468	0.715	1.538	0.620
FRS	w/o Lapla	25.256	0.924	3.065	0.610
	w/o SenB	25.111	0.923	3.051	0.610
	Remove	25.040	0.920	3.051	0.611
	Instead	16.111	0.721	1.597	0.610
ALL		25.623	0.929	3.081	0.610

Table 2. Ablation for the FRR and FRS modules and all their sub-modules. The **Remove** indicates deletion from the full model, and the **Instead** denotes replacement with a CBM group of equivalent parameters and receptive fields.

4.4. Ablation Study

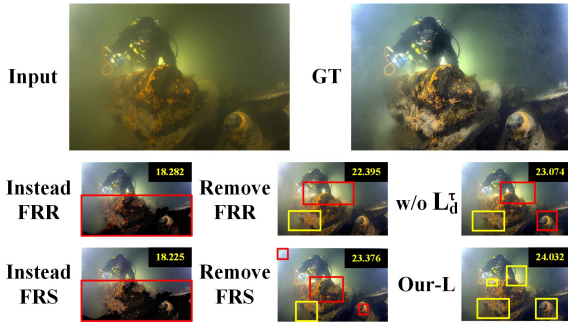


Figure 7. Visual comparison of ablation study on UIEB V90. The red box shows the error enhancements, the yellow box shows the excellent enhancements and the PSNR score is in the upper right corner of the image.

4.4.1 Effectiveness of FRR

Our FRR module is designed to reduce noise and balance the colors in images. As depicted in Figure 5 (a) and (b), it effectively removes color casts but introduces motion blur. The results of the ablation study in Table 2 reveal that FRR not only improves feature repair and reconstruction but also enhances performance, increasing PSNR by 0.7 and SSIM by 0.007.

4.4.2 Effectiveness of FRS

The FRS module, which employs fixed-weight Laplacian convolution, excels at extracting low-frequency features and reducing artifacts. Table 2 demonstrates that FRS significantly boosts PSNR and SSIM by 11.5 and 0.2, respectively, surpassing other convolution groups. The ‘Remove’ experiment further validates the role of FRS in enhancing

model performance. Additionally, experiments involving the Laplacian convolution and smoothing module confirm the effectiveness of our approach. A comparison between Figure 5 (b) and 7 (c) clearly illustrates the FRS module’s ability to eliminate blurring and artifacts, particularly at object edges.

Loss	PSNR	SSIM	UIQM	UCIQE
w/o L_1	25.133	0.931	3.053	0.608
w/o L_{ssim}	25.201	0.912	3.125	0.611
w/o L_d^τ	25.404	0.927	3.064	0.610
ALL	25.623	0.929	3.081	0.610

Table 3. Evaluating combinations of Loss functions.

4.4.3 Effectiveness of L_d^τ

Our L_d^τ is designed to preserve advanced features such as contrast and light balance, expedite network training, and assist the network in avoiding local optima. As demonstrated in Tables 3 and 4, an increase in the weight of L_d^τ correlates with a rise in UIQM values, indicating its effective role in guiding contrast and light balance. Moreover, the PSNR value is 0.24 dB higher when using L_d^τ compared to not using it, illustrating its ability to guide the network more effectively towards the global optimum. As shown in Figure 7, L_d^τ also allows the images recovered by our model to outperform the light and contrast balance of the ground truth to some extent.

Weight	PSNR	SSIM	UIQM	UCIQE
0.00	25.133	0.931	3.053	0.608
0.35	25.623	0.929	3.081	0.610
0.70	25.522	0.928	3.093	0.607
1.00	24.742	0.925	3.112	0.605
1.50	17.030	0.736	3.377	0.590

Table 4. Assessing the impact of L_d^τ weight variations.

5. Conclusion

In this study, we propose a lightweight and efficient enhancement network for underwater image enhancement, improves visual quality, particularly in noise reduction, effectively boosting the model’s generalizability and adaptability. Our proposed dynamic gradient guidance strategy effectively controls the restoration effect, providing a novel perspective on the interpretability of UIE tasks. Comparative experiments demonstrate that our method surpasses the Semi-UIR method (CVPR’23): achieving a higher PSNR of 25.1 (a 3.3% improvement), 88.3% fewer parameters, and a 61.7% increase in computational efficiency, making it more suitable for underwater exploration.

References

- [1] Liangyu Chen, Xiaojie Chu, Xiangyu Zhang, and Jian Sun. Simple baselines for image restoration. In *ECCV*, pages 17–33. Springer, 2022. 1, 6, 7
- [2] Xiang Chen, Hao Li, Mingqiang Li, and Jinshan Pan. Learning a sparse transformer network for effective image deraining. In *CVPR*, pages 5896–5905, 2023. 1
- [3] Runmin Cong, Wenyu Yang, Wei Zhang, Chongyi Li, Chunle Guo, Qingming Huang, and Sam Kwong. Pagan: Physical model-guided underwater image enhancement using gan with dual-discriminators. *TIP*, 2023. 3
- [4] Yuning Cui, Yi Tao, Wenqi Ren, and Alois Knoll. Dual-domain attention for image deblurring. In *AAAI*, pages 479–487, 2023. 1
- [5] Zhenqi Fu, Wu Wang, Yue Huang, Xinghao Ding, and Kai-Kuang Ma. Uncertainty inspired underwater image enhancement. In *ECCV*, pages 465–482. Springer, 2022. 1, 6, 7
- [6] Chunle Guo, Qixin Yan, Saeed Anwar, Runmin Cong, and Chongyi Li. Image dehazing transformer with transmission-aware 3d position embedding. In *CVPR*, pages 5812–5820, 2022. 1
- [7] Chunle Guo, Ruiqi Wu, Xin Jin, Linghao Han, Zhi Chai, Weidong Zhang, and Chongyi Li. Underwater ranker: Learn which is better and how to be better. In *AAAI*, pages 720–709, 2023. 3
- [8] Shirui Huang, Keyan Wang, Huan Liu, Jun Chen, and Yunsong Li. Contrastive semi-supervised learning for underwater image restoration via reliable bank. In *CVPR*, pages 18145–18155, 2023. 1, 6, 7
- [9] Shirui Huang, Keyan Wang, Huan Liu, Jun Chen, and Yunsong Li. Contrastive semi-supervised learning for underwater image restoration via reliable bank. In *CVPR*, pages 18145–18155, 2023. 3
- [10] Kui Jiang, Zhongyuan Wang, Peng Yi, Chen Chen, Baojin Huang, Yimin Luo, Jiayi Ma, and Junjun Jiang. Multi-scale progressive fusion network for single image deraining. In *CVPR*, pages 8346–8355, 2020. 1
- [11] Kui Jiang, Zhongyuan Wang, Peng Yi, Chen Chen, Zheng Wang, Xiao Wang, Junjun Jiang, and Chia-Wen Lin. Rain-free and residue hand-in-hand: A progressive coupled network for real-time image deraining. *TIP*, 30:7404–7418, 2021. 1
- [12] Xin Jin, Jia-Wen Xiao, Ling-Hao Han, Chunle Guo, Ruixun Zhang, Xialei Liu, and Chongyi Li. Lighting every darkness in two pairs: A calibration-free pipeline for raw denoising. In *ICCV*, pages 13275–13284, 2023. 1
- [13] Jari Korhonen and Junyong You. Peak signal-to-noise ratio revisited: Is simple beautiful? In *2012 Fourth International Workshop on Quality of Multimedia Experience*, pages 37–38. IEEE, 2012. 7
- [14] Chongyi Li, Jichang Guo, Runmin Cong, Yanwei Pang, and Bo Wang. Underwater image enhancement by dehazing with minimum information loss and histogram distribution prior. *TIP*, 25(22):5664–5677, 2016. 3
- [15] Chongyi Li, Chunle Guo, Wenqi Ren, Runmin Cong, Junhui Hou, Sam Kwong, and Dacheng Tao. An underwater image enhancement benchmark dataset and beyond. *TIP*, 29:4376–4389, 2019. 1, 2, 7
- [16] Chongyi Li, Saeed Anwar, and Fatih Porikli. Underwater scene prior inspired deep underwater image and video enhancement. *PR*, 98:107038, 2020. 2, 6, 7
- [17] Chongyi Li, Saeed Anwar, Junhui Hou, Runmin Cong, Chunle Guo, and Wenqi Ren. Underwater image enhancement via medium transmission-guided multi-color space embedding. *TIP*, 30:4985–5000, 2021. 1, 3, 6, 7
- [18] Chongyi Li, Chunle Guo, Ling-Hao Han, Jun Jiang, Ming-Ming Cheng, Jinwei Gu, and Chen Change Loy. Low-light image and video enhancement using deep learning: A survey. *TPAMI*, 2021. 1
- [19] Chongyi Li, Chunle Guo, and Chen Change Loy. Learning to enhance low-light image via zero-reference deep curve estimation. *TPAMI*, 2021. 1
- [20] Hanyu Li, Jingjing Li, and Wei Wang. A fusion adversarial underwater image enhancement network with a public test dataset. *arXiv preprint arXiv:1906.06819*, 2019. 7
- [21] Jie Li, Katherine A Skinner, Ryan M Eustice, and Matthew Johnson-Roberson. Watergan: Unsupervised generative network to enable real-time color correction of monocular underwater images. *IEEE Robotics and Automation letters*, 3(1):387–394, 2017. 2, 3
- [22] Philipp Lindenberger, Paul-Edouard Sarlin, and Marc Pollefeys. LightGlue: Local Feature Matching at Light Speed. In *ICCV*, 2023.
- [23] Risheng Liu, Xin Fan, Ming Zhu, Minjun Hou, and Zhongxuan Luo. Real-world underwater enhancement: Challenges, benchmarks, and solutions under natural light. *TCSVT*, 30(12):4861–4875, 2020. 7
- [24] Yun Liu, Zhongsheng Yan, Sixiang Chen, Tian Ye, Wenqi Ren, and Erkang Chen. Nighthazeformer: Single nighttime haze removal using prior query transformer. In *ACMMM*, pages 4119–4128, 2023. 1
- [25] Ben Mildenhall, Pratul P. Srinivasan, Rodrigo Ortiz-Cayon, Nima Khademi Kalantari, Ravi Ramamoorthi, Ren Ng, and Abhishek Kar. Local light field fusion: Practical view synthesis with prescriptive sampling guidelines. *TOG*, 2019.
- [26] Karen Panetta, Chen Gao, and Sos Agaian. Human-visual-system-inspired underwater image quality measures. *IEEE Journal of Oceanic Engineering*, 41(3):541–551, 2015. 7
- [27] Lintao Peng, Chunli Zhu, and Liheng Bian. U-shape transformer for underwater image enhancement. *TIP*, 2023. 3
- [28] Yan-Tsung Peng, Keming Cao, and Pamela C Cosman. Generalization of the dark channel prior for single image restoration. *TIP*, 27(6):2856–2868, 2018. 3
- [29] Yuhui Quan, Xiaoheng Tan, Yan Huang, Yong Xu, and Hui Ji. Image desnowing via deep invertible separation. *TCSVT*, 2023. 1, 2
- [30] Katherine A. Skinner, Eduardo Iscar Ruland, and M. Johnson-Roberson. Automatic color correction for 3d reconstruction of underwater scenes. In *IEEE International Conference on Robotics and Automation*, 2017.
- [31] Wei Song, Yan Wang, Dongmei Huang, Antonio Liotta, and Cristian Perra. Enhancement of underwater images with statistical model of background light and optimization of trans-

- mission map. *IEEE Transactions on Broadcasting*, 66(1): 153–169, 2020. 3, 6, 7
- [32] Wei Song, Yan Wang, Dongmei Huang, Antonio Liotta, and Cristian Perra. Enhancement of underwater images with statistical model of background light and optimization of transmission map. *IEEE Transactions on Broadcasting*, 66(1): 153–169, 2020. 3
- [33] Shangquan Sun, Wenqi Ren, Tao Wang, and Xiaochun Cao. Rethinking image restoration for object detection. *Advances in Neural Information Processing Systems*, 35:4461–4474, 2022. 2
- [34] Yudong Wang, Jichang Guo, Huan Gao, and Huihui Yue. Uiecc²-net: Cnn-based underwater image enhancement using two color space. *Signal Processing: Image Communication*, 96:116250, 2021. 1, 6, 7
- [35] Yinglong Wang, Chao Ma, and Jianzhuang Liu. Smartassign: Learning a smart knowledge assignment strategy for deraining and desnowing. In *CVPR*, pages 3677–3686, 2023. 1
- [36] Zhou Wang, Alan C Bovik, Hamid R Sheikh, and Eero P Simoncelli. Image quality assessment: from error visibility to structural similarity. *TIP*, 13(4):600–612, 2004. 5, 7
- [37] Rui-Qi Wu, Zheng-Peng Duan, Chun-Le Guo, Zhi Chai, and Chongyi Li. Ridcp: Revitalizing real image dehazing via high-quality codebook priors. In *CVPR*, pages 22282–22291, 2023. 1
- [38] Yuhui Wu, Chen Pan, Guoqing Wang, Yang Yang, Jiwei Wei, Chongyi Li, and Heng Tao Shen. Learning semantic-aware knowledge guidance for low-light image enhancement. In *CVPR*, pages 1662–1671, 2023. 1
- [39] Miao Yang and Arcot Sowmya. An underwater color image quality evaluation metric. *TIP*, 24(12):6062–6071, 2015. 7
- [40] Yongcan Yu, Jianhu Zhao, Chao Huang, and Xi Zhao. Treat noise as domain shift: Noise feature disentanglement for underwater perception and maritime surveys in side-scan sonar images. *IEEE Transactions on Geoscience and Remote Sensing*, 61:1–15, 2023. 3
- [41] Syed Waqas Zamir, Aditya Arora, Salman Khan, Munawar Hayat, Fahad Shahbaz Khan, and Ming-Hsuan Yang. Restormer: Efficient transformer for high-resolution image restoration. In *CVPR*, pages 5728–5739, 2022. 1, 6, 7
- [42] Dan Zhang, Zongxin He, Xiaohuan Zhang, Zhen Wang, Wenyi Ge, Taian Shi, and Yi Lin. Underwater image enhancement via multi-scale fusion and adaptive color-gamma correction in low-light conditions. *Engineering Applications of Artificial Intelligence*, 126:106972, 2023. 3
- [43] Dehuan Zhang, Chenyu Wu, Jingchun Zhou, Weishi Zhang, Chaolei Li, and Zifan Lin. Hierarchical attention aggregation with multi-resolution feature learning for gan-based underwater image enhancement. *Engineering Applications of Artificial Intelligence*, 125:106743, 2023. 1, 3, 6, 7
- [44] Dehuan Zhang, Jingchun Zhou, Weishi Zhang, Zifan Lin, Jian Yao, Kemal Polat, Fayadh Alenezi, and Adi Alhudhaif. Rex-net: A reflectance-guided underwater image enhancement network for extreme scenarios. *Expert Systems with Applications*, page 120842, 2023. 1, 6, 7
- [45] Kaihao Zhang, Tao Wang, Wenhan Luo, Wenqi Ren, Björn Stenger, Wei Liu, Hongdong Li, and Ming-Hsuan Yang. Mc-blur: A comprehensive benchmark for image deblurring. *TCSVT*, 2023. 1
- [46] Weidong Zhang, Peixian Zhuang, Hai-Han Sun, Guohou Li, Sam Kwong, and Chongyi Li. Underwater image enhancement via minimal color loss and locally adaptive contrast enhancement. *TIP*, 31:3997–4010, 2022. 3
- [47] Naishan Zheng, Man Zhou, Yanmeng Dong, Xiangyu Rui, Jie Huang, Chongyi Li, and Feng Zhao. Empowering low-light image enhancer through customized learnable priors. In *ICCV*, pages 12559–12569, 2023. 1
- [48] Jingchun Zhou, Dehuan Zhang, Wenqi Ren, and Weishi Zhang. Auto color correction of underwater images utilizing depth information. *IEEE Geoscience and Remote Sensing Letters*, 19:1–5, 2022. 6
- [49] Jingchun Zhou, Boshen Li, Dehuan Zhang, Jieyu Yuan, Weishi Zhang, Zhanchuan Cai, and Jinyu Shi. Ugif-net: An efficient fully guided information flow network for underwater image enhancement. *IEEE Transactions on Geoscience and Remote Sensing*, 61:1–17, 2023. 1
- [50] Jingchun Zhou, Qian Liu, Qiuping Jiang, Wenqi Ren, Kin-Man Lam, and Weishi Zhang. Underwater camera: improving visual perception via adaptive dark pixel prior and color correction. *IJCV*, pages 1–19, 2023. 1
- [51] Jingchun Zhou, Jiaming Sun, Weishi Zhang, and Zifan Lin. Multi-view underwater image enhancement method via embedded fusion mechanism. *Engineering Applications of Artificial Intelligence*, 121:105946, 2023. 1, 6, 7
- [52] Shanchen Zhou, Chongyi Li, and Chen Change Loy. Lednet: Joint low-light enhancement and deblurring in the dark. In *ECCV*, pages 1–17, 2022. 1
- [53] Qi Zhu, Man Zhou, Naishan Zheng, Chongyi Li, Jie Huang, and Feng Zhao. Exploring temporal frequency spectrum in deep video deblurring. In *ICCV*, pages 12428–12437, 2023. 1